

Analysis of structural, morphological and magnetic properties of diluted magnetic semiconductor ZnO:Eu obtained by combustion reaction

(Análise das propriedades estruturais, morfológicas e magnéticas do semicondutor magnético diluído ZnO:Eu obtido via reação de combustão)

D. B. Maia^{1*}, R. A. Raimundo^{2,3}, T. A. Passos¹, R. A. Torquato¹

¹Federal University of Paraíba, Department of Materials Engineering, João Pessoa, PB, Brazil

²Federal University of Paraíba, Graduate Program in Mechanical Engineering, João Pessoa, PB, Brazil

³Federal University of Rio Grande do Norte, Department of Theoretical and Experimental Physics, Natal, RN, Brazil

Abstract

Eu-doped semiconductor matrix of ZnO at concentrations of 0.05 and 0.10 mols was synthesized by combustion reaction, using zinc nitrate, europium nitrate, and urea as fuel. In order to analyze the effect of europium concentration and sintering on the structure, band gap, magnetic and morphological properties of ZnO, the samples were sintered at 1100 °C for 30 min and analyzed before and after sintering via X-ray diffraction, ultraviolet and visible spectroscopy, vibrant sample magnetometry, and scanning electron microscopy. From the results obtained, it was found that there was the formation of the semiconductor phase ZnO and also a second-phase (Eu₂O₃). It was observed that the samples before and after sintering presented band gap values within the semiconductor range and ferromagnetism at room temperature.

Keywords: diluted magnetic semiconductor, combustion reaction, zinc oxide, europium.

Resumo

Matriz semicondutora de ZnO, dopada com Eu nas concentrações de 0,05 e 0,10 mols, foi sintetizada por reação de combustão utilizando nitrato de zinco, nitrato de európio e ureia como combustível. No intuito de analisar o efeito da concentração de európio e da sinterização na estrutura, band gap, propriedades magnéticas e morfológicas do ZnO, as amostras foram sinterizadas a 1100 °C por 30 min e analisadas antes e após sinterização por difração de raios X, espectroscopia na região do ultravioleta e visível, magnetometria de amostra vibrante e microscopia eletrônica de varredura. A partir dos resultados obtidos, constatou-se que houve formação da fase semicondutora ZnO e também de uma segunda fase (Eu₂O₃). Observou-se que as amostras antes e após a sinterização apresentaram valores de band gap dentro da faixa dos semicondutores e ferromagnetismo à temperatura ambiente.

Palavras-chave: semicondutor magnético diluído, reação de combustão, óxido de zinco, európio.

INTRODUCTION

Spintronics, or spin electronics, is a new field of microelectronics based on the simultaneous manipulation of electron charge and spin, which are responsible, respectively, for the transmission and storage of information [1]. The aim of this emerging science is to enable the combination of communication, memory, and processing on a single device, creating a new generation of smaller, faster, and with lower power consumption than current ones, operating on the basis of the combination of conventional microelectronics and spin-dependent effects [2]. Ideal material for spintronics application has ferromagnetism above room temperature, and semiconductor and ferromagnetic property with the possibility of spin manipulation [3]. However, there is

an important challenge related to the composition of semiconductors that hinders the simultaneous control of the spin and electron. Semiconductors consist of semimetals, elements that do not have considerable magnetic properties, since they have no magnetic momentum. So, in order for these materials to acquire magnetic behavior, it is necessary to introduce ions with magnetic characteristics along the semiconductor matrix lattice. The material resulting from the replacement of the cations of the semiconductor matrix by these magnetic ions is called diluted magnetic semiconductor (DMS) [4, 5].

Several semiconductors were analyzed for the purpose of obtaining DMSs, among them are manganese-doped gallium arsenide (GaAs:Mn) [6], manganese-doped gallium nitride (GaN:Mn) [7], manganese-doped indium arsenide (InAs:Mn) [8], and zinc oxide doped with nickel (ZnO:Ni), manganese (ZnO:Mn), and cobalt (ZnO:Co) [9-11]. Among these materials, zinc oxide (ZnO) has become one of the most studied DMS-based systems because it has interesting

*daniel.bmaia@hotmail.com

<https://orcid.org/0000-0001-8043-6362>

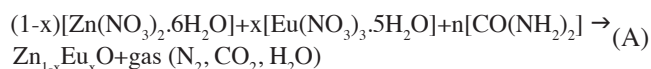
semiconductor and optical properties, characteristics that make it ideal for application in electronic and optoelectronic devices such as UV light emitters, varistors, piezoelectric transducers, and gas sensors [4]. The main properties of this intrinsic semiconductor consist of a wide and direct gap (~3.37 eV), a high exciton binding energy (60 meV), and a good electronic mobility [12]. In addition, several studies have reported ferromagnetic behavior above ambient temperature by doping transition metal ions with 3d valence orbitals such as iron [13], manganese, cobalt, and nickel [14], or rare earths with 4f valency orbitals [15], obtaining DMSs. Among rare earth ions, europium (Eu) has stood out due to its good magnetic momentum (~6.9 μB) [16].

There are several techniques reported in the literature that can be used to obtain DMSs, such as the sol-gel method, coprecipitation, Pechini method, aqueous solution, and hydrothermal method [17-21]. However, most of these techniques present certain obstacles to the large-scale production of powders, since they require expensive reagents and often have toxicity, complicated synthesis steps, high temperatures, and long reaction times [22]. In addition to these methods, there is the combustion reaction synthesis, which has emerged as a promising alternative for the production of DMS systems for being a fast, effective, low-cost method, simple, performed in few steps, and without the need for sophisticated equipment [23]. This technique consists of an exothermic chemical reaction between metal nitrates and an organic fuel, usually urea. A peculiarity that makes this process distinct from others is that the heat required to conduct the chemical reaction is provided by the reaction itself, due to the decomposition of the mixture between the reagents, and not by an external source. The heat released during the reaction can reach high temperatures, promoting the elimination of impurities and the crystallization of the formed product, an agglomerated dry powder with high-purity and chemical homogeneity [24]. Thus, the present study aimed to perform a comparative analysis of the structure, morphology, and magnetic properties before and after sintering of the europium ion-doped zinc oxide at different concentrations (0.05 and 0.10 mol Eu) obtained by combustion reaction synthesis, aiming to produce a DMS for application in spintronic devices.

EXPERIMENTAL

The synthesis by combustion reaction had, as precursors, zinc nitrate hexahydrate $[\text{Zn}(\text{NO}_3)_2 \cdot 6\text{H}_2\text{O}]$ and europium nitrate pentahydrate $[\text{Eu}(\text{NO}_3)_3 \cdot 5\text{H}_2\text{O}]$, and as organic fuel urea $[\text{CO}(\text{NH}_2)_2]$. All reagents were manufactured by Sigma-Aldrich, USA. The reaction was performed in order to obtain the $\text{Zn}_{1-x}\text{Eu}_x\text{O}$ system with $x = 0$ (pure ZnO), 0.05, and 0.10 mol Eu, whose stoichiometry was defined based on the total valence of oxidizing (nitrate) and reducing (urea) reagents, according to the theory of propellants and explosives [25]. According to this theory, the reaction considers the amount of fuel (n) that should be used to balance the reaction and the quantities of the other reagents determined by the product to

be obtained, as follows:



According to the thermochemical concepts of propelling chemistry [25], elements such as H, C, Eu, and Zn are considered reducing elements, O is an oxidizing element, and N has a neutral valence, so that the corresponding valence for each element is Eu +3, N 0, H +1, O -2, Zn +2, and C +4. Thus, the stoichiometric composition of the redox mixture to release maximum energy during the reaction requires $10+6n=0$ or $n=1.67$ mols of urea for pure ZnO, $-10.75+6n=0$ or $n=1.71$ mols of urea for the $\text{Zn}_{0.95}\text{Eu}_{0.05}\text{O}$ system, and $-10.5+6n=0$ or $n=1.75$ mols of urea for the $\text{Zn}_{0.9}\text{Eu}_{0.1}\text{O}$ system. After defining the stoichiometry of the reaction, the amount of reagents in each sample was determined, and the redox mixture obtained was submitted to direct heating in an electrical resistance furnace until it reached autoignition. Then, the reaction product was calcined in the air atmosphere in a muffle furnace (EDG Equip., EDG 3P-S), at 500 °C for 5 min in order to promote crystallization of the zinc oxide phase without the presence of secondary phases; later, it was de-agglomerated in a 325 mesh (45 μm) sieve. After that, the powders were formed into pellets to be sintered. Forming was performed by uniaxial pressing at 249.7 MPa for 1 min. Subsequently, the pellets were sintered in a tubular furnace (Quimis, Q320M) under vacuum (10^{-3} mbar) at 1100 °C, with a holding time of 30 min, a heating rate of 10 °C/min, and cooled inside the furnace to room temperature.

The samples were characterized by X-ray diffraction (XRD) using a diffractometer (Bruker, D2 Phaser), in the 2θ range of 30-75° with a 0.02° step, with 2 °/min scanning rate, $\text{CuK}\alpha$ radiation ($\lambda=1.5418 \text{ \AA}$), 30 kV voltage, and 10 mA current. Ultraviolet and visible (UV-vis) spectroscopy was performed in reflectance mode with a spectrophotometer (Shimadzu, UV-2550) in the wavelength range from 200 to 800 nm. Magnetic measurements were performed via a vibrant sample magnetometer (VSM, EG&G, VSM 4500). The hysteresis cycles were obtained at 27 °C with a maximum magnetic field of 10 kOe at a rate of 5 Oe/s for all measurements. The material morphology was analyzed by scanning electron microscopy (SEM, Zeiss, Auriga 40).

RESULTS AND DISCUSSION

Fig. 1a shows the X-ray diffraction (DRX) patterns of pure ZnO and ZnO:Eu systems. The diffractograms of the ZnO:Eu systems were compared with that of pure ZnO, and the peaks concerning the hexagonal wurtzite phase (P63mc space group) of zinc oxide (ZnO) remained unchanged. The peaks indicated by Z corresponded to zinc oxide whose reflection planes were the same as the wurtzite structure found in the literature (ICSD 01-075-0576). It was also observed that only the system with $x=0.10$ mol of Eu exhibited a small peak at $2\theta 28.7^\circ$, characteristic of the europium oxide phase (Eu_2O_3 , ICSD 01-074-1988). According to the literature [26-28], Eu_2O_3 is a very stable phase whose appearance was

due to the difficult solubilization of europium in the ZnO crystal lattice, since, besides the much larger ionic radius of the Eu^{3+} (0.98 Å) than Zn^{2+} (0.77 Å), there is a preference for Eu^{3+} ions in octahedral sites, which they occupy in the cubic structure of Eu_2O_3 , while the position of zinc ions in the wurtzite is tetrahedral. X-ray diffraction analysis of undoped ZnO revealed some low intensity peaks in this material, indicated with an asterisk, but which were not observed in the ZnO:Eu systems. These peaks located at 2θ 27.0°, 28.3°, and 33.1° in the undoped ZnO were not found in the crystallographic files; therefore, since this material was obtained in laboratory via combustion reaction, these peaks were considered as residues of the precursor decomposition during synthesis. Fig. 1b shows a detailed view of the reflection plane (101), the most intense diffraction peak for the ZnO wurtzite structure. It was evident that the peak of the ZnO:Eu systems shifted to smaller angles relative to pure ZnO, indicating that the Eu^{3+} ions have successfully replaced

the Zn^{2+} ions in the ZnO structure, since the ionic radius of the Eu^{3+} ion is much larger than Zn^{2+} , in order to cause an increase in the lattice parameters. This was confirmed by the results of the lattice parameters and the volume of the unit cell of pure ZnO and ZnO:Eu systems (Table I), calculated by the UnitCell program, using a nonlinear least squares method [29]. It was expected that the peaks of the sample with 0.10 mol of Eu would suffer a greater displacement to smaller angles in relation to the one with 0.05 mol of Eu, since the concentration of europium was higher; however, this was not observed. Ivetić et al. [30] reported the decrease in lattice parameters with increasing europium concentration in Eu-doped ZnO nanoparticles obtained via combustion reaction. As mentioned, the 0.10 mol Eu-doped sample had second-phase formation (Eu_2O_3), which explains this result, since, possibly, the Eu^{3+} ions in this system were introduced into the ZnO crystal lattice, replacing Zn^{2+} , but also became segregated on the surface as a secondary phase, suppressing

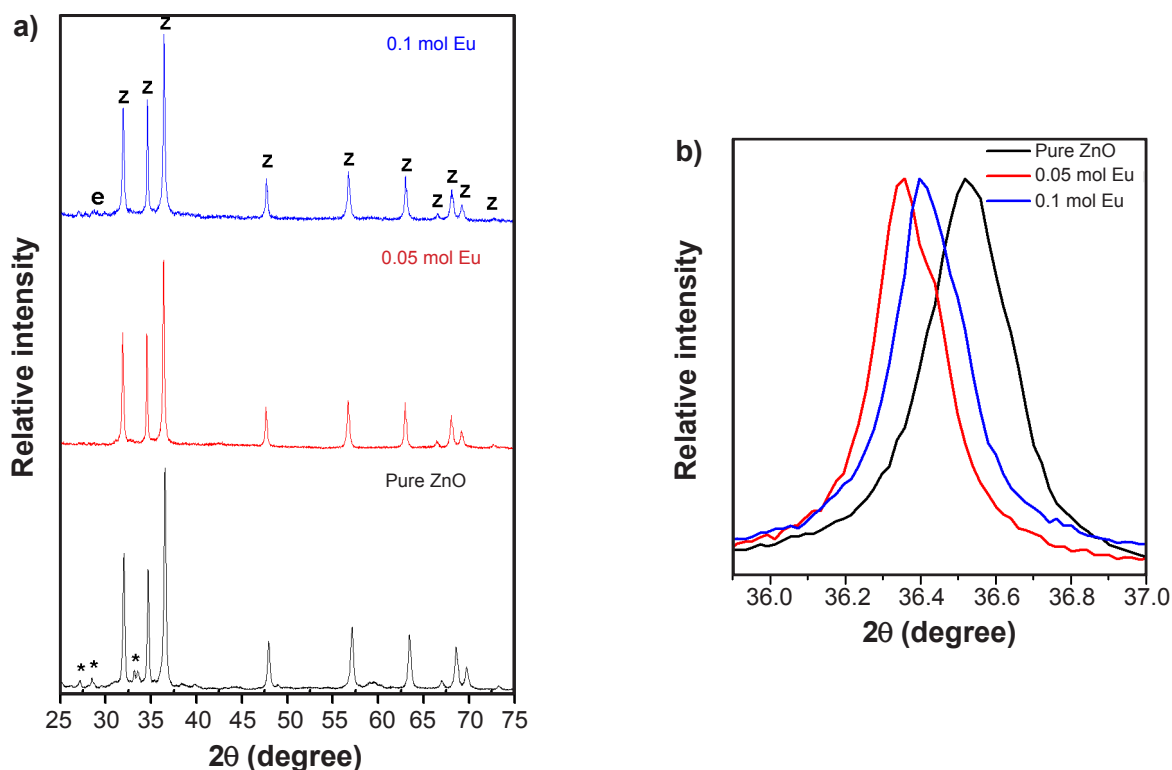


Figure 1: X-ray diffractograms of pure ZnO and ZnO:Eu powders prepared by combustion reaction method (a) and enlargement of the reflection of the plane (101) (b).

[Figura 1: Difratogramas de raios X dos pós de ZnO puro e ZnO:Eu preparados pelo método de reação de combustão (a) e ampliação da reflexão do plano (101) (b).]

Table I - Lattice parameters (a, b, c) and volume (V) of unit cell of the samples.

[Tabela I - Parâmetros de rede (a, b, c) e volume (V) de célula unitária das amostras.]

Sample	a=b (Å)	c (Å)	c/a	V (Å ³)
ICSD 01-075-0576	3.242	5.194	1.602	47.277
Pure ZnO	3.221	5.165	1.603	46.413
0.05 mol Eu	3.245	5.198	1.602	47.400
0.10 mol Eu	3.242	5.195	1.602	47.301

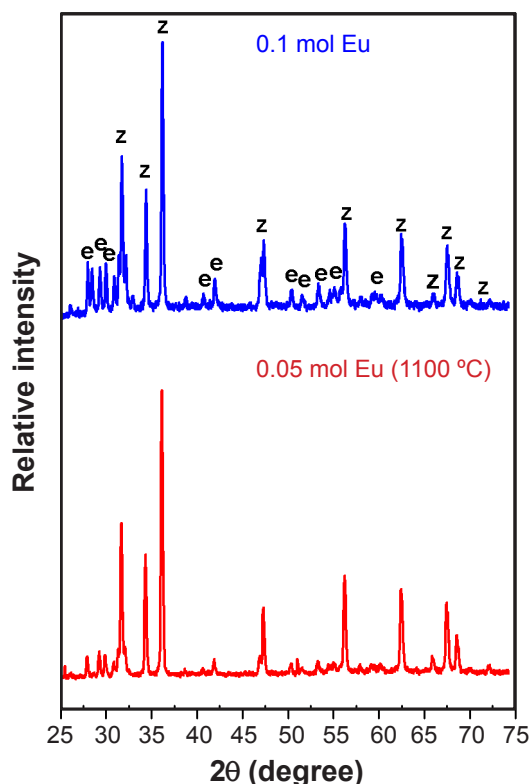


Figure 2: X-ray diffractograms of ZnO:Eu systems sintered at 1100 °C.

[Figura 2: Difratoformas de raios X dos sistemas ZnO:Eu sinterizados a 1100 °C.]

part of the effect of the ions introduced into the crystal lattice, causing a reduction of the lattice parameters.

Fig. 2 shows the X-ray diffractograms of the ZnO:Eu systems after sintering. The formation of the Eu_2O_3 phase, observed before sintering only in the 0.10 mol Eu sample with cubic structure, in this condition appeared in the two samples with monoclinic structure (space group C2/m, ICSD 00-034-0072). This transition in the structure of Eu_2O_3 is discussed in the literature [31], which reports that this oxide is present in the cubic structure at temperatures below 1050 °C and has a monoclinic structure at high temperatures, between 1100 and 2040 °C, a behavior consistent with the results demonstrated.

The band gap value of the samples was determined by ultraviolet and visible region (UV-vis) spectroscopy using the method proposed by Tauc [32]. According to this method, the band gap (E_g) is given by:

$$(\alpha \cdot hv)^n = A \cdot (hv - E_g) \quad (B)$$

where α is the absorbance, hv is the photon energy (eV), and A is a proportionality parameter. The value of index n depends on the type of electronic transition of the material, assuming a value of 1/2 for indirect transition and 2 for direct transitions, the latter being used for zinc oxide. Thus, the value of E_g is given by the intersection of the extrapolation of the linear region of the graph generated by the Eq. B with the abscissa [33]. The results obtained from UV-vis spectroscopy of the ZnO:Eu systems before and

after sintering are shown in Figs. 3a and 3b, respectively. Comparing with the theoretical value of E_g of zinc oxide (~ 3.37 eV) [11], it was noted that due to the europium doping, the band gap was reduced, but the values were still within the semiconductor range. The reason for this reduction was probably due to changes in the electronic structure of ZnO due to europium dilution in its lattice [34]. These changes may occur due to the deformation of the structure with the introduction of larger Eu^{3+} ions into the ZnO lattice and also due to variations in carrier concentrations, since rare earth impurities, such as europium, when introduced into the ZnO structure are found in the 3+ oxidation state, where they donate two electrons to stabilize the bond with neighboring oxygen atoms, while the third electron fills the bottom of the ZnO conduction band [35, 36].

The hysteresis cycles of pure ZnO and powdered and sintered ZnO:Eu systems are shown in Figs. 4 and 5, respectively. The cycle of pure ZnO was characteristic of a diamagnetic material. The remanent magnetization (M_r)

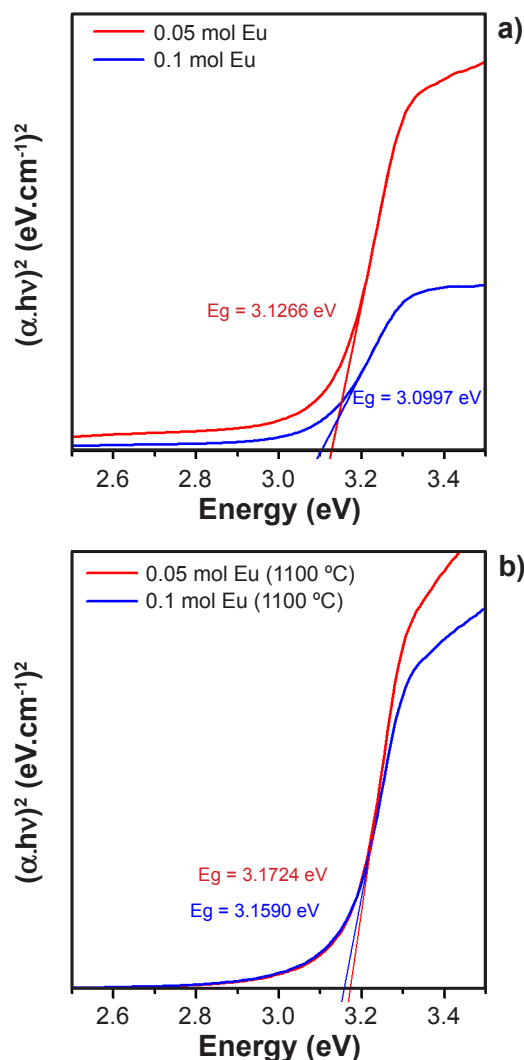


Figure 3: Tauc plots showing the band gaps of ZnO:Eu systems in powder form (a) and after sintering (b).

[Figura 3: Gráficos de Tauc mostrando band gaps dos sistemas ZnO:Eu em forma de pó (a) e após sinterização (b).]

and coercive field (H_c) values of the powdered and sintered ZnO:Eu systems are shown in Table II. The powdered samples exhibited a weak ferromagnetic behavior, evidenced by the small hysteresis in relatively low fields, characteristic of ceramic materials, and the low M_r values [37, 38]. The origin of ferromagnetism in ZnO doped with Eu is a highly discussed topic. It is known that the possibility of the appearance of this phenomenon associated with the formation of a europium oxide secondary phase, such as EuO and Eu_2O_3 , is ruled out, since EuO is ferromagnetic only at very low temperatures, having a Curie temperature (T_c) of $-204\text{ }^\circ\text{C}$, and Eu_2O_3 is paramagnetic at $27\text{ }^\circ\text{C}$ [39]. Furthermore, according to the X-ray diffraction analysis, EuO was not detected in both samples and Eu_2O_3 appeared only in the 0.10 mol Eu sample, but both samples had

ferromagnetism at room temperature, confirming that this magnetic behavior should not be associated with this phase. Therefore, the origin of ferromagnetism is expected to be related to the exchange interactions between the magnetic moments of Eu^{3+} ions in the structure and to the increase in the amount of intrinsic defects, such as oxygen and zinc vacancies. Ling-Feng et al. [40] studied the effects of europium doping on ZnO magnetic properties and found that samples containing oxygen vacancies had higher ferromagnetism stability compared to samples without oxygen vacancies, leading to the conclusion that samples under scarce oxygen conditions tend to present higher ferromagnetism than the same samples under richer oxygen conditions. The origin of ferromagnetism related to oxygen vacancies is due to the formation of bound magnetic polarons (BMP) [41]. Thus, the higher the concentration of Eu^{3+} dopant and the density of oxygen vacancies, the higher the production of BMPs along the lattice and, consequently, the stronger the ferromagnetic behavior of the material. Therefore, the material with 0.10 mol of Eu was expected to have better ferromagnetic results compared to 0.05 mol of Eu because it had higher europium concentration, but this did not occur. The explanation for this result is probably due to the formation of the Eu_2O_3 phase in the 0.10 mol Eu sample, reported in the X-ray diffraction analysis, since this oxide is paramagnetic at room temperature, promoting a linearization of the hysteresis curve of this system.

It was noticed that all the magnetic parameters of the sintered samples showed lower values than those of the samples in powder form. With the sintering process, it was expected that the amount of oxygen vacancies would tend to increase, since the energy supplied to the pellets with their heating promotes the release of oxygen, which would make the ferromagnetic behavior of the sintered samples stronger than those in the powder condition; however, this was not observed. Probably, these values of the magnetic

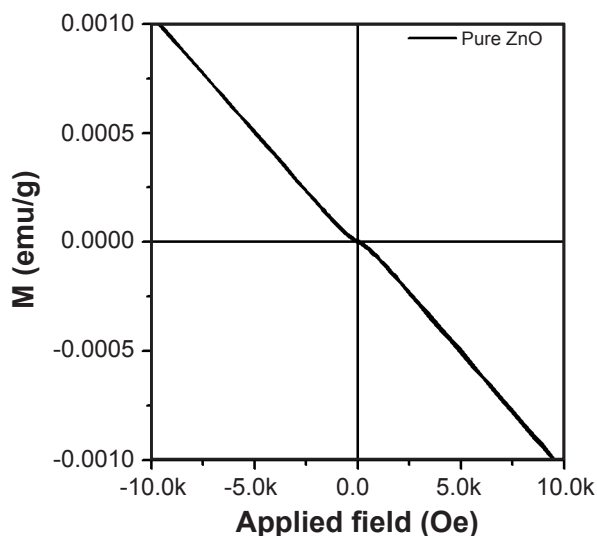


Figure 4: Magnetization curve of pure ZnO powder. [Figura 4: Curva de magnetização do pó de ZnO puro.]

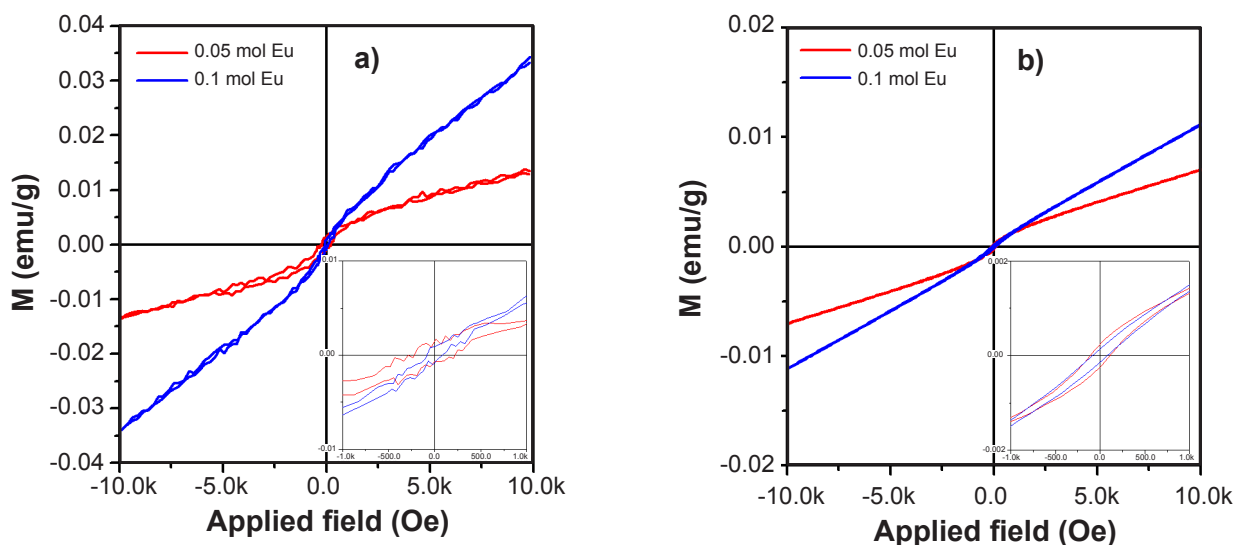


Figure 5: Magnetization curves of ZnO:Eu systems in powder form (a) and after sintering (b). The inset show a magnification of the curves. [Figura 5: Curvas de magnetização dos sistemas ZnO:Eu em forma de pó (a) e após sinterização (b). A inserção mostra uma ampliação das curvas.]

Table II - Magnetic parameters of ZnO:Eu systems in powder and sintered form.

[Tabela II - Parâmetros magnéticos dos sistemas ZnO:Eu em forma de pó e sinterizados.]

Sample	M_r (emu/g)	H_c (Oe)
0.05 mol Eu (powder)	1.447×10^{-3}	221.32
0.10 mol Eu (powder)	8.730×10^{-4}	84.41
0.05 mol Eu (1100 °C)	2.484×10^{-4}	107.14
0.10 mol Eu (1100 °C)	1.557×10^{-4}	79.76

M_r : remanent magnetization; H_c : coercive field.

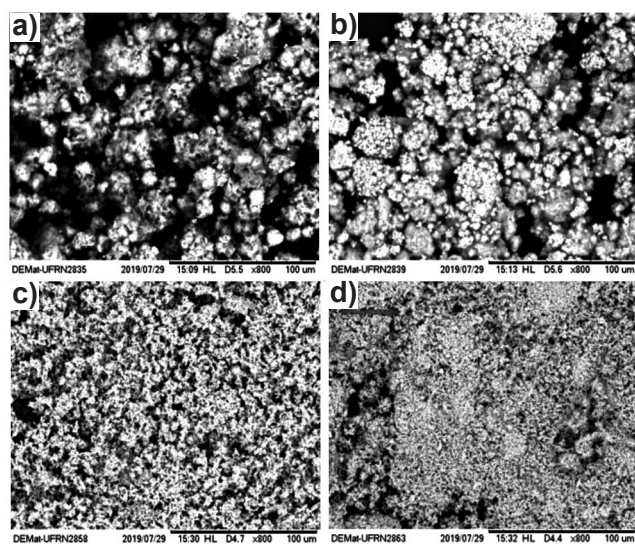


Figure 6: SEM micrographs of doped samples with 0.05 mol Eu (a,c) and 0.10 mol Eu (b,d) in powder form (a,b) and after sintering (c,d).

[Figura 6: Micrografias obtidas por microscopia eletrônica de varredura das amostras dopadas com 0,05 mol Eu (a,c) e 0,10 mol de Eu (b) em forma de pó (a,b) e após sinterização (c,d).]

parameters lower than those of the samples in powder form were due to the formation of the Eu_2O_3 phase, identified in the analysis by X-ray diffraction of both samples. With the segregation of this paramagnetic phase, there was a decrease in interactions between free electrons donated by Eu^{3+} ions and oxygen vacancies, weakening the ferromagnetism of the sintered samples. Another explanation for this result is given by the material morphology. Fig. 6 shows SEM images of the two samples before and after the sintering. The magnetic properties are dependent on the movement process of the domain walls, which, in turn, is influenced by the grain size and the presence of microstructural defects, such as porosity. The influence of grain size is the fact that the larger the grain size, it is easier to move the walls, requiring less energy to magnetize and demagnetize the material. Therefore, samples with larger grains are expected to have low coercivity (H_c) [42, 43]. On the other hand, porosity tends to increase H_c , since the increase in the amount of pores makes it difficult to move the walls, requiring a higher field to rotate the magnetic dipoles contained within the domain walls [44]. Thus, considering that the sintering process, in

addition to reducing the amount of these pores making the material denser, promoted an increase in the grain size, it is expected that there is a significant decrease in the remanent magnetization (M_r) and coercive field (H_c), which in fact occurred.

CONCLUSIONS

In this study, the synthesis of doped zinc oxide with different europium concentrations, obtaining the $\text{Zn}_{1-x}\text{Eu}_x\text{O}$ system with $x=0.05$ and 0.10 mol, was successfully performed via combustion reaction. According to the XRD results of the powder samples, it was found that a single-phase material was produced only for the 0.05 mol Eu doped sample, while in both sintered samples there was a second-phase formation (Eu_2O_3). From the results of the UV-vis spectroscopy, it was observed that all samples, before and after sintering, presented lower band gap values relative to the theoretical value of pure zinc oxide, but they remained within the semiconductor band, fulfilling one of the requirements for obtaining a DMS (diluted magnetic semiconductor), i.e., the semiconductor property. According to VSM analysis, the presence of ferromagnetism at room temperature was evident for both Eu concentrations under powder and sintered material conditions. Thus, europium-doped zinc oxide obtained via combustion reaction is a suitable material for the production of diluted magnetic semiconductors for spintronic application as it meets all requirements such as ambient temperature ferromagnetism and semiconductor property, and ferromagnetism with the possibility of spin manipulation.

ACKNOWLEDGMENT

The authors acknowledge CNPq Scientific Initiation Program (PIBIC) for its financial support.

REFERENCES

- [1] V.A. Ivanov, T.G. Aminov, V.M. Novotortsev, V.T. Kalinnikov, Russ. Chem. Bull. **53**, 11 (2004) 2357.
- [2] S.A. Wolf, D.D. Awschalon, R.A. Buhrman, J.M. Daughton, S. von Molnár, M.L. Roukes, A.Y. Chtchelkanova, D.M. Treger, Science **294**, 5546 (2001) 1488.
- [3] M. Diaconu, H. Schmidt, H. Hochmuth, M. Lorenz, G. Benndorf, D. Spemann, A. Setzera, P. Esquinazia, A. Pöppl, H. von Wencksterna, K.-W. Nielsen, R. Gross, H. Schmid, W. Mader, G. Wagner, M. Grundmann, J. Magn. Mater. **307**, 2 (2006) 212.
- [4] S.J. Pearton, D.P. Norton, K. Ip, Y.W. Heo, T. Steiner, Prog. Mater. Sci. **50**, 3 (2005) 293.
- [5] M.C. Prestgard, G.P. Siegel, A. Tiwari, Adv. Mater. Lett. **5**, 5 (2014) 242.
- [6] H. Ohno, A. Shen, F. Matsukura, A. Oiwa, A. Endo, S. Katsumoto, Y. Iye, Appl. Phys. Lett. **69**, 3 (1996) 363.
- [7] K.H. Baik, R.M. Frazier, G.T. Thaler, C.R. Abernathy, S.J. Pearton, J. Kelly, R. Rairigh, A.F. Hebard, W. Tang, M.

- Stavola, J.M. Zavada, Appl. Phys. Lett. **83**, 26 (2003) 5458.
- [8] H. Ohno, H. Munekata, T. Penney, S. Von Molnar, L.L. Chang, Phys. Rev. Lett. **68**, 17 (1992) 2664.
- [9] D.A. Schwartz, K.R. Kittilstved, D.R. Gamelin, Appl. Phys. Lett. **85**, 8 (2004) 1395.
- [10] P. Sharma, A. Gupta, K.V. Rao, F.J. Owens, R. Sharma, R. Ahuja, J.M.O. Guillen, B. Johansson, G.A. Gehring, Nat. Mater. **2**, 10 (2003) 673.
- [11] J. Wojnarowicz, S. Kusnieruk, T. Chudoba, S. Gierlotka, W. Lojkowski, W. Knoff, M.I. Lukasiewicz, B.S. Witkowski, A. Wolska, M.T. Klepka, T. Story, M. Godlewski, Beilstein J. Nanotechnol. **6** (2015) 1957.
- [12] C. Mayrinck, E. Raphael, J.L. Ferrari, M.A. Schiavon, Rev. Virt. Quím. **6**, 5 (2014) 1185.
- [13] A. Goktas, I.H. Mutlu, Y. Yamada, Superlattices Microstruct. **57** (2013) 139.
- [14] R.A. Torquato, “Síntese por reação de combustão de ZnO dopado com Mn²⁺, Co²⁺ e Ni²⁺ para obtenção de semicondutores magnéticos diluídos (SMD)”, Doct. Thesis, UFPB, Campina Grande (2011).
- [15] T. Dietl, Nat. Mater. **9**, 12 (2010) 965.
- [16] F. Benosman, Z. Dridi, Y. Al-Douri, B. Bouhafs, Int. J. Mod. Phys. B **30**, 31 (2016) 1650225.
- [17] S. Husain, F. Rahman, N. Ali, P.A. Alvi, J. Optoelectron. Eng. **1**, 1 (2013) 28.
- [18] R. Saleh, N.F. Djaja, S.P. Prakoso, J. Alloys Compd. **546** (2013) 48.
- [19] C. Sánchez, C. Paucar, A. Mosquera, J.E. Rodríguez, A. Gómez, O. Morán, Superlattices Microstruct. **52**, 2 (2012) 249.
- [20] D. Wu, M. Yang, Z. Huang, G. Yin, X. Liao, Y. Kang, X. Chen, H. Wang, J. Colloid Interface Sci. **330**, 2 (2009) 380.
- [21] L. Wu, Y. Wu, L.Ü. Wei, Physica E Low Dimens. Syst. Nanostruct. **28**, 1 (2005) 76.
- [22] A. Franco Jr, H.V.S. Pessoni, M.P. Soares, J. Magn. Mater. **355** (2014) 325.
- [23] K.C. Patil, S.T. Aruna, T. Mimani, Curr. Opin. Solid State Mater. Sci. **6**, 6 (2002) 507.
- [24] Y. Zhang, G.C. Stangle, J. Mater. Res. **9**, 8 (1994) 1997.
- [25] S.R. Jain, K.C. Adiga, V.P. Verneker, Combust. Flame **40** (1981) 71.
- [26] M. Lorke, T. Frauenheim, A.L. Da Rosa, Phys. Rev. B **93**, 11 (2016) 115132.
- [27] S. Kumar, R. Prakash, V.K. Singh, Rev. Adv. Sci. Eng. **4**, 4 (2015) 247.
- [28] B.S. Barros, P.S. Melo, L. Gama, S. Alves-Jr, E. Fagury-Neto, R.H.G.A. Kiminami, A.C.F.M. Costa, Cerâmica **51**, 317 (2005) 63.
- [29] T. Holland, S. Redfern, “UnitCell”, <http://www.ccp14.ac.uk> (2006).
- [30] T.B. Ivetić, M.R. Dimitrievska, I.O. Gúth, L.R. Đačanin, S.R. Lukić-Petrović, J. Res. Phys. **36**, 1 (2012) 43.
- [31] W.A. Ross, R.L. Gibby, J. Am. Ceram. Soc. **57**, 1 (1974) 46.
- [32] J. Tauc, Mater. Res. Bull. **3**, 1 (1968) 37.
- [33] M. Meinert, G. Reiss, J. Phys. Condens. Matter **26**, 11 (2014) 115503.
- [34] A.F.V. Da Fonseca, R.L. Siqueira, R. Landers, J.L. Ferrari, N.L. Marana, J.R. Sambrano, F.A. La Porta, M.A. Schiavon, J. Alloys Compd. **739** (2018) 939.
- [35] G. Caroen, W.V.M. Machado, J.F. Justo, L.V.C. Assali, Appl. Phys. Lett. **102**, 6 (2013) 62101.
- [36] P. Pandey, R. Kurchania, F.Z. Haque, J. Adv. Phys. **3**, 2 (2014) 104.
- [37] A. Franco Jr, H.V.S. Pessoni, M.P. Soares, J. Magn. Mater. **355** (2014) 325.
- [38] V.C.S. Diniz, B.B. Dantas, A.R. Figueiredo, D.R. Cornejo, A.C.F.M. Costa, Cerâmica **61**, 359 (2015) 298.
- [39] H. Yoon, J.H. Wu, J.H. Min, J.S. Lee, J.S. Ju, Y.K. Kim, J. Appl. Phys. **111**, 7 (2012) 7B523.
- [40] Q. Ling-Feng, H. Qing-Yu, J. Xiao-Fang, X. Zhen-Chao, Z. Chun-Wang, Physica B Condens. Matter **530** (2018) 133.
- [41] R.L. Aggarwal, J.K. Furdyna, S. Von Molnar (Eds.), “Diluted magnetic (semimagnetic) semiconductors”, Mater. Res. Soc. Symp. Proc. **89**, MRS, Pittsburgh (1987).
- [42] A.C.F.M. Costa, M.R. Morelli, R.H.G.A. Kiminami, Cerâmica **49**, 311 (2003) 168.
- [43] F.L. Zabotto, A.J. Gualdi, J.A. Eiras, A.J.A.D. Oliveira, D. Garcia, Mater. Res. **15**, 3 (2012) 428.
- [44] R.N. Faria, L.F. Lima, *Introdução ao magnetismo dos materiais*, Ed. Livr. Fís., S. Paulo (2005).

(Rec. 30/10/2019, Rev. 08/03/2020, Ac. 14/03/2020)